JGR Oceans

RESEARCH ARTICLE
10.1029/2024JC020903

Special Collection:
The Arctic Ocean's changing Beaufort Gyre

Quantifying Drivers of Seasonal and Interannual Variability of Dissolved Oxygen in the Canada Basin Mixed Layer

Ashley Arroyo[1], **Mary-Louise Timmermans**[1], **and Mike DeGrandpre**[2]

[1]Department of Earth and Planetary Sciences, Yale University, New Haven, CT, USA, [2]Department of Chemistry and Biochemistry, University of Montana, Missoula, MT, USA

Key Points:

- Spatial and seasonal distributions of O_2 concentrations in the Canada Basin mixed layer are linked to the seasonal evolution of sea ice
- Modeled fluxes suggest brine rejection and meltwater dilution during sea ice melt/formation dominate seasonal variability of mixed layer O_2
- Decreases in mixed-layer O_2 during winter (over 2007–2019) suggest outgassing, likely driven by changes in the wintertime sea ice pack

Supporting Information:

Supporting Information may be found in the online version of this article.

Correspondence to:

A. Arroyo,
ashley.arroyo@yale.edu

Citation:

Arroyo, A., Timmermans, M.-L., & DeGrandpre, M. (2024). Quantifying drivers of seasonal and interannual variability of dissolved oxygen in the Canada Basin mixed layer. *Journal of Geophysical Research: Oceans*, *129*, e2024JC020903. https://doi.org/10.1029/2024JC020903

Received 10 JAN 2024
Accepted 20 JUN 2024

Author Contributions:

Formal analysis: Ashley Arroyo
Funding acquisition: Mary-Louise Timmermans
Investigation: Ashley Arroyo
Methodology: Mary-Louise Timmermans
Supervision: Mary-Louise Timmermans
Visualization: Ashley Arroyo
Writing – original draft: Ashley Arroyo
Writing – review & editing: Mary-Louise Timmermans, Mike DeGrandpre

Abstract Analysis of dissolved oxygen (O_2) in the Arctic's surface ocean provides insights into gas transfer between the atmosphere-ice-ocean system, water mass dynamics, and biogeochemical processes. In the Arctic Ocean's Canada Basin mixed layer, higher O_2 concentrations are generally observed under sea ice compared to open water regions. Annual cycles of O_2 and O_2 saturation, increasing from summer through spring and then sharply declining to late summer, are tightly linked to sea ice cover. The primary fluxes that influence seasonal variability of O_2 are modeled and compared to Ice-Tethered Profiler O_2 observations to understand the relative role of each flux in the annual cycle. Findings suggest that sea ice melt/growth dominates seasonal variations in mixed layer O_2, with minor contributions from vertical entrainment and atmospheric exchange. While the influence of biological activity on O_2 variability cannot be directly assessed, indirect evidence suggests relatively minor contributions, although with significant uncertainty. Past studies show that O_2 molecules are expelled from sea ice during brine rejection; sea ice cover can then inhibit air-sea gas exchange resulting in winter mixed layers that are super-saturated. Decreasing mixed layer O_2 concentrations and saturation levels are observed during winter months between 2007 and 2019 in the Canada Basin. Only a minor portion of the decreasing trend in wintertime O_2 can be attributed to decreased solubility. This suggests the O_2 decline may be linked to more efficient air-sea exchange associated with increased open water areas in the winter sea ice pack that are not necessarily detectable via satellite observations.

Plain Language Summary Dissolved oxygen (O_2) is a valuable ocean property that allows us to better understand the exchange of gases between the different ocean layers, sea ice, and atmosphere, and the physical and biological processes that control its variability. Understanding how and why O_2 concentrations in the Arctic Ocean mixed layer vary spatially and seasonally is crucial for interpreting its evolution over timescales of years to decades that are influenced by global warming. We use physical and thermodynamical relationships to model the main factors that influence O_2 concentrations in the mixed layer of the Arctic Ocean's Canada Basin, which we compare to observations made by Ice-Tethered Profilers. Model results indicate that seasonal variations in O_2 concentrations are dominated by the effects of sea ice growth and melt. Other processes that modulate mixed layer O_2, including air-sea exchange and ocean mixing, have a lesser influence. Between 2007 and 2019, mixed-layer O_2 has decreased in winter months, which we attribute to more openings in the sea-ice pack during wintertime in the Canada Basin.

1. Introduction

The Arctic Ocean's Canada Basin mixed layer serves as the connection between the overlying sea ice cover, and the stratified waters of the halocline, where this stratification inhibits the flux of subsurface heat to the underside of sea ice (e.g., Aagaard et al., 1981; Toole et al., 2010). Mixed layer properties in this region are strongly seasonally varying, and depend largely on the annual cycle of local sea ice retreat. The winter is characterized by relatively deep and salty mixed layers resulting from sea ice growth and vertical mixing, with temperatures near the freezing point (Figures 1a and 1b). In contrast, summertime mixed layers, with a stronger stratification across their base, are shallow and fresh, due to river runoff accumulation and sea ice melt, and can have temperatures above the freezing point (Figures 1a–1c) (Peralta-Ferriz & Woodgate, 2015; Toole et al., 2010).

O_2 concentration in the surface ocean in contact with the atmosphere is influenced by O_2 solubility (i.e., the maximum amount of O_2 that can be dissolved in seawater), which is a function of temperature, salinity, and

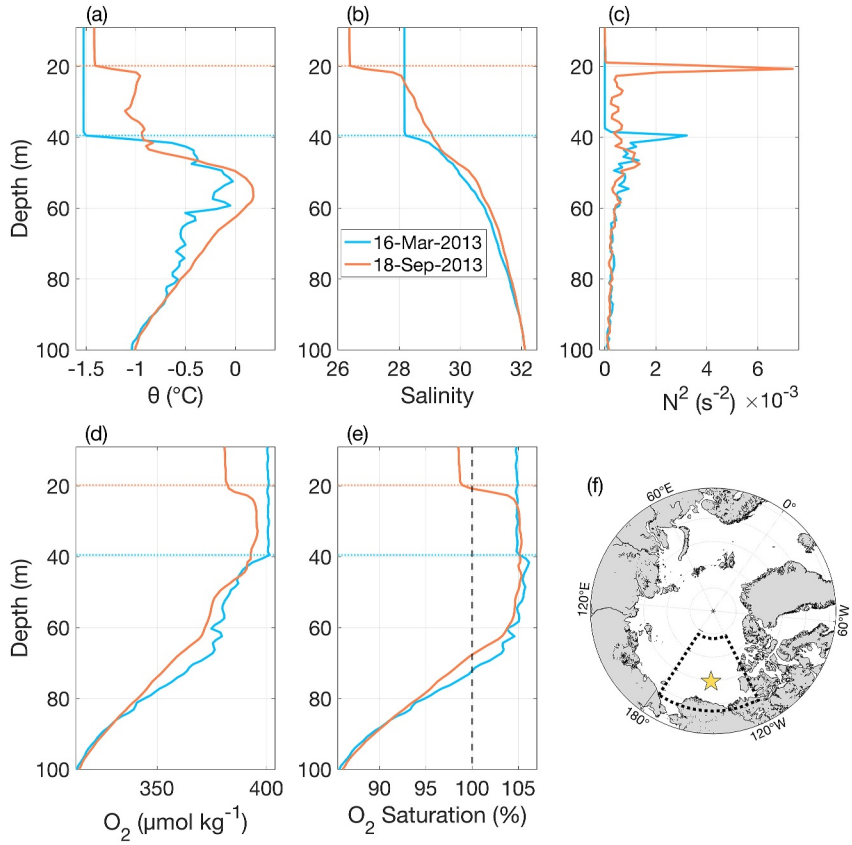

Figure 1. Typical profiles of parameters in the Canada Basin: (a) Potential temperature, (b) salinity, (c) buoyancy frequency (N^2), (d) O_2, and (e) O_2 percent saturation in the summertime (orange) and wintertime (blue) are shown. The orange and blue dashed lines indicate mixed-layer depths in the summer and winter profiles, respectively. The black dashed line in (e) indicates 100% saturation. A map of the region is shown in (f), where the location of the profiles is shown as a yellow star and the area encompassed by the map in Figure 2a is delineated by dashed lines.

atmospheric pressure (Garcia & Gordon, 1992). Biological and physical processes can give rise to deviations from 100% saturation. During sea ice formation, O_2 (among other solutes, including salt and other dissolved gases) is expelled from the crystal lattice into the underlying ocean mixed layer (Glud et al., 2002; Top et al., 1985). For example, O_2 rich brine has been shown to be generated by enhanced sea-ice production in polynyas (e.g., Dmitrenko et al., 2015). High O_2 concentrations and super-saturation can arise when sea ice cover inhibits O_2 accumulated during ice growth from outgassing to the atmosphere (see e.g., Timmermans et al., 2010). While efficient atmospheric gas exchange drives equilibration, the presence of a thick sea ice pack with few openings or leads impedes this, which leads to minimal gas exchange through the Arctic winter (e.g., Poisson & Chen, 1987; Rutgers van der Loeff et al., 2014). Conversely, sea ice melt reduces O_2 concentrations in the mixed layer due to addition of low O_2 meltwater. As a result of sea ice growth and decay, winter mixed layers are characterized by generally high (super-saturated) O_2 concentrations (Figures 1d and 1e), while O_2 summer mixed layers have relatively low O_2, near or below 100% saturation (Figures 1d and 1e).

The fresh and O_2 depleted summer mixed layers are isolated from the subsurface due to the strong stratification of the seasonal halocline (Figure 1c). Beneath the summer mixed layer, there is a sharp transition to a local O_2 maximum (Figure 1d), which can be 20–40 m thick and coincides with the remnant winter mixed layer (Timmermans et al., 2010). This subsurface O_2 maximum is typically super-saturated, resembling wintertime saturation levels (Figure 1e), suggesting that it results from O_2 accumulation during wintertime sea ice growth that is subsequently trapped and preserved under strong stratification throughout the year. Timmermans et al. (2010) also noted the potential role of in situ primary production in the development of the sub-surface O_2 maximum. This O_2 maximum typically does not persist past December/January, as the waters are mixed through (either mechanically by shear-driven mixing or convectively by brine rejection). After these seasonal features are mixed

up, warm waters with lower O_2 sourced from the Pacific Ocean reside directly below the mixed layer. During periods of vertical ocean mixing, the waters beneath the mixed layer can become entrained into the mixed layer, altering O_2 concentrations based on the O_2 gradient between the sub-surface and the mixed layer (see e.g., Gordon et al., 1984; Körtzinger et al., 2008).

Other processes, including biology and lateral advection also influence O_2 concentrations in the mixed layer. Biological processes, that is, photosynthesis and respiration, produce and consume O_2, respectively. Moreau et al. (2015) note the importance of bacterial respiration in regulating under-ice O_2 concentrations during periods of sea ice growth and melt, while Glud et al. (2014) suggest that sea-ice meltwater dilution has a much larger influence on O_2 concentrations than biological activity. Waters that are laterally advected into the Canada Basin (i.e., sourcing from rivers or the Pacific Ocean) also influence O_2 concentrations in the mixed layer (Islam et al., 2017; see their Figure 9a), as O_2 concentrations often reflect the signatures of their source regions (Falkner et al., 2005). However, the specific influences of various processes on O_2 in the mixed layer are not well constrained. It is important to gain insights into the mechanisms governing O_2 variability over seasonal and interannual timescales to understand the dynamics of gas transfer between sea ice, the ocean, and the atmosphere, specifically relating to recent sea ice decline.

Here, we analyze observations in the Canada Basin (Figure 1f) from Ice-Tethered Profilers (ITPs) sampling between 2007 and 2019 and hydrographic data from annual Joint Ocean Ice Study/Beaufort Gyre Observing System (JOIS/BGOS) expeditions between 2003 and 2022, to quantify the drivers of seasonal and interannual variability of O_2 in the Canada Basin mixed layer. In the next section, we describe the data sources and provide expressions used in a one-dimensional modeling approach that quantifies the contributions of various processes to the mixed layer O_2 budget on seasonal timescales. In Section 3, we explore the spatial variability of O_2 in the Canada Basin mixed layer and its relation to the sea ice cover. Section 4 describes and compares the seasonal cycle of O_2 and that of sea ice growth and melt and other processes. Section 5 outlines and explains the results and limitations of the one-dimensional model to understand the dominant processes driving the seasonal cycle of O_2. The evolution of O_2 in the Canada Basin mixed layer between 2007 and 2019 is analyzed in Section 6. We summarize and discuss our results in Section 7.

2. Data and Methods

2.1. Hydrographic Data

Ship data from annual JOIS/BGOS expeditions (http://www.whoi.edu/beaufortgyre), which occur sometime between July and October from 2003 to 2022, are analyzed to diagnose mechanisms driving spatial variability in mixed layer O_2 in the Canada Basin. These data are high vertical resolution profiles of ocean properties, including temperature, salinity, and dissolved oxygen, collected via conductivity-temperature-depth (CTD)/Rosette casts which included a SeaBird Electronics 43 (SBE-43) dissolved oxygen sensor. The initial accuracy of the SBE-43 sensor is stated to be ±2% of saturation (Sea-Bird Electronics Inc, 2018). The O_2 measurements are binned into 1 dbar averages, and are calibrated using the SeaBird Inc. lab calibration procedure along with measurements from the Niskin bottles equipped on the CTD/Rosette. The accuracy of the final calibrated O_2 data is determined by the standard deviation with O_2 samples from the Niskin bottles, where the standard deviation across all samples in a yearly expedition is typically about ±3.5 μmol kg^{-1} (Arroyo et al., 2023).

2.2. Ice-Tethered Profiler Data

ITPs are autonomous sampling systems that are comprised of a surface buoy that sits on an ice floe and a wire rope tether suspended below that supports a conductivity-temperature-depth (CTD) profiler (Krishfield et al., 2008; Toole et al., 2011) (http://www.whoi.edu/itp). The CTD unit profiles along the wire from approximately 7–760 m depth at a speed of ∼25 cm s^{-1} (sampling at a frequency of 1 Hz), returning data with 25 cm vertical resolution that are bin-averaged into 1-db pressure bins (Krishfield et al., 2008). The ITPs have drift speeds typically ranging from 10 to 30 cm s^{-1} and return 2–6 profiles per day, providing data with horizontal resolution on the order of a few kilometers (Krishfield et al., 2008). A subset of ITPs are additionally equipped with Sea-Bird Electronics O_2 sensors (SBE 43, see Sea-Bird Electronics Inc. (2023)), which measure the flux of O_2 that diffuses through a membrane. O_2 concentrations are computed from SBE 43 sensor data using the Seabird algorithm which is based on that of Owens and Millard (1985). Data processing methods are described by Timmermans et al. (2010), and include corrections for downcasts influenced by the wake of the CTD, sensor drift, and sensor calibration using

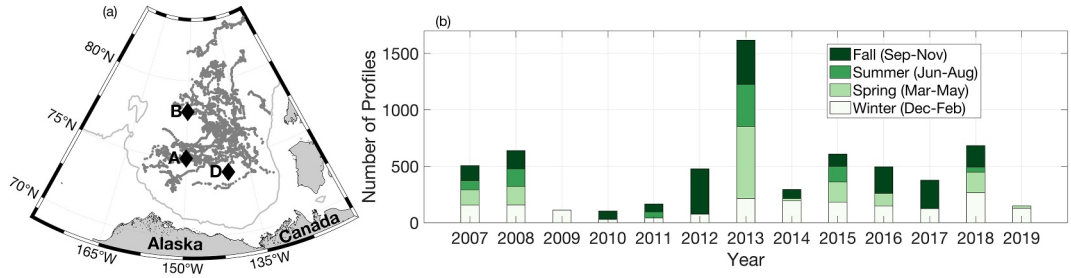

Figure 2. (a) Drift tracks in the Canada Basin of 21 ITPs equipped with O_2 sensors used in this analysis (gray). BGOS mooring sites are indicated by black diamonds. The 500 m isobath is shown in gray. (b) The temporal distribution of ITP profiles in each year partitioned by seasons (see legend).

hydrographic O_2 data on deep potential isotherms during the sampling duration of the ITP. In this study, we use the fully processed data (Level 3; see http://www.whoi.edu/itp/data) from 21 ITPs equipped with O_2 sensors that drifted throughout the Canada Basin, in the region within 72–84°N and 160–120°W between January 2007 and March 2019. The drift tracks and temporal distribution of ITP profiles are shown in Figure 2.

Mixed-layer depth is computed from each ITP profile as the first depth at which the potential density exceeds that of the shallowest measurement by 0.1 kg m^{-3} (e.g., Toole et al., 2010).

2.3. Sea Ice Draft Data

Three moorings (locations shown in Figure 2a) equipped with Upward Looking Sonar (ULS) are recovered and deployed annually as part of the Beaufort Gyre Observing System (BGOS; http://www.whoi.edu/beaufortgyre). These moorings provide measurements of sea ice draft (accurate to ∼±10 cm). We use daily averaged sea ice draft over 2007–2019 to characterize ice growth and decay at each of the moorings (Figure S1 in Supporting Information S1). We consider weekly moving means, since the records from each of the three moorings show good agreement on weekly time scales (R^2 of 0.73 across the 3 moorings). Uncertainty is estimated as the standard deviation across moorings.

A few of the ITPs analyzed here were deployed on the same floe with Ice Mass Balance Buoys (IMBs; Richter-Menge et al. (2006)), which return information on sea-ice thickness. However, reliable measurements of both O_2 and ice-thickness from the same floe at the same time were sparse. Therefore, for the present study we limit ice-thickness information to the mooring data.

2.4. Other Supporting Data

Sea ice concentration (SIC) data with daily, 25 km resolution are from the National Atmospheric and Oceanic Administration/National Snow and Ice Data Center (NOAA/NSIDC) Climate Data Record of Passive Microwave Sea Ice Concentration, Version 4 (https://nsidc.org/data/g02202/). The wind and sea level pressure data were retrieved from the fifth generation European Centre for Medium Range Weather Forecasting (ECMWF) reanalysis data set (ERA5; Hersbach et al. (2020)), which provides hourly estimates of atmospheric parameters with 0.25 by 0.25° horizontal resolution. Lindsay et al. (2014) evaluated the performance of seven reanalysis products in the Arctic region, and found that ERA-Interim (the precursor to the improved ERA5; Hersbach et al. (2020); Belmonte Rivas and Stoffelen (2019)) was among the most consistent with independent observations for several key parameters, including 10 m wind fields for which biases were generally less than 0.5 m s^{-1}. They found that sea level pressure (SLP) data had good agreement across the products (Lindsay et al., 2014). Daily second moments of the wind speed are computed by taking the mean of the winds at 10 m height (U_{10}) squared (see Wanninkhof, 2014), and used to compute gas transfer velocities. Daily averages of SLP are used to account for variations in atmospheric pressure in the computation of O_2 solubility. For the SIC, wind, and SLP data, we use the grid cell measurements closest in location and time to the ITP and hydrographic observations.

2.5. One-Dimensional Modeling

To gain insight into the mechanisms driving seasonal variability of mixed layer O_2, we modeled the O_2 variability due to each influencing factor and compare model results to observations. The variability of mixed layer O_2 is modeled as a sum of the following factors:

$$\Delta O_2^T = \Delta O_2^I + \Delta O_2^A + \Delta O_2^E + \Delta O_2^B + \Delta O_2^L, \quad (1)$$

where O_2^I, ΔO_2^A, ΔO_2^E, ΔO_2^B, and ΔO_2^L represent changes in mixed layer O_2 due to sea ice growth and melt, atmospheric transfer (which includes a parametrization for bubble injection), vertical entrainment, biology (photosynthesis and respiration), and lateral advection, respectively. Each of these terms is described in detail in the following sub-sections.

2.5.1. Ice Growth and Melt

Sea ice growth and melt influences O_2 concentrations in the mixed layer due to O_2 exclusion and meltwater dilution, respectively. To quantify the influences of sea ice growth and melt on mixed layer O_2 concentrations, we used a mass balance model, similar to that used by DeGrandpre et al. (2019), who modeled the influence of sea ice processes on carbon cycle parameters. The O_2 mass balance (per unit area) from one time step ($t-1$) to the next (t) is as follows:

$$\rho_t h_t O_{2_t} + \rho^{ice} h_t^{ice} {O_2}^{ice} = \rho_{t-1} h_{t-1} O_{2_{t-1}} + \rho^{ice} h_{t-1}^{ice} {O_2}^{ice}, \quad (2)$$

Quantities with no superscripts refer to mixed-layer properties, and the ice superscripts refer to ice values. h is mixed-layer depth, h^{ice} is ice draft, and O_2 and ρ are mixed-layer averaged O_2 and density, respectively. Sea ice density, ρ^{ice}, is taken to be 900 kg m^{-3}. Top et al. (1985) found that 52 ± 1% of O_2 is rejected during sea ice formation, which gives ${O_2}^{ice} = 0.48\, O_{2_{t-1}}$, however, we note this parameter is highly variable depending on ice age, type, and salinity (Cox & Weeks, 1983). As a result, there may be additional uncertainty associated with this term. Equation 2 can be used with conservation of mass $\left(\rho_t h_t + \rho^{ice} h_t^{ice} = \rho_{t-1} h_{t-1} + \rho^{ice} h_{t-1}^{ice}\right)$ to solve for mixed layer O_2 as follows:

$$O_{2_t} = O_{2_{t-1}} + \frac{\rho^{ice}}{\rho_t h_t}\left(h_t^{ice} - h_{t-1}^{ice}\right)\left(O_{2_{t-1}} - {O_2}^{ice}\right), \quad (3)$$

so that the change in O_2 as a result of sea ice draft change, Δh^{ice}, may be written as

$$\Delta O_2^I = \frac{\rho^{ice} \Delta h^{ice}}{\rho_t h_t}\left(O_{2_{t-1}} - {O_2}^{ice}\right). \quad (4)$$

The largest source of uncertainty in ΔO_2^I is the uncertainty in Δh^{ice} (with the combined uncertainty in the other parameters, except that of ${O_2}^{ice}$ which is not well constrained, being relatively small), which is estimated from the standard deviation of h^{ice} across the three moorings.

2.5.2. Atmospheric Gas Exchange

To calculate the atmospheric flux of O_2 (F_{atm}) into or out of the mixed layer at time t, we use the following expression:

$$F_{atm} = \left[k_{O_2}\left(O_{2sol_t} - O_{2_t}\right)\right]\left(1 - SIC_t\right). \quad (5)$$

F_{atm} is weighted linearly by open water area following the findings of Butterworth and Miller (2016), and flux goes to zero with 100% ice cover. SIC is the sea ice concentration (from 0 to 1) and $O_{2_{sol}}$ is mixed layer averaged O_2 solubility. $O_{2_{sol}}$ is computed using the equations of Garcia and Gordon (1992), and corrected for variations in

atmospheric pressure following the methods of Wu et al. (2022). $O_{2_{sol}}$ is also corrected for the effects of bubble injection, following the methods of Woolf and Thorpe (1991). The gas transfer velocity, k_{O_2}, is computed as

$$k_{O_2} = 0.251 < U_{10}^2 > \left(\frac{Sc}{660}\right)^{-0.5} \quad (6)$$

(Wanninkhof, 2014), where $<U_{10}^2>$ is the daily second moment of wind speed at 10 m height. Sc is the Schmidt number, which is the ratio of the kinematic viscosity of seawater to the molecular diffusion coefficient of O_2, and is computed following Wanninkhof (2014) using mixed layer temperature values, and O_2 specific coefficients in seawater. Positive F_{atm} indicates a flux from the atmosphere into the mixed layer. We express changes in O_2 concentration as

$$\Delta O_2^A = \frac{\Delta t}{h_t}[k_{O_2}(O_{2sol_{t-1}} - O_{2_{t-1}})](1 - SIC_{t-1}), \quad (7)$$

where Δt is the time step in days.

The uncertainty of ΔO_2^A is computed using the uncertainties associated with U_{10}, k_{O_2}, SIC, and the bubble injection correction in the computation of $O_{2_{sol}}$. Wanninkhof (2014) compared various empirical formulations for the expression for k_{O_2} and deduce that a 20% uncertainty in the value of k_{O_2} estimated by Equation 6 is appropriate. In addition to this uncertainty, the uncertainty of U_{10} is computed using the spread of the ensemble members of ERA5 wind data components. The uncertainty in the SIC is computed using the standard deviation across the surrounding grid cells (details are provided here https://nsidc.org/data/g02202/versions/4). While Woolf and Thorpe (1991) do not explicitly state an uncertainty for their bubble supersaturation parameterization, Liang et al. (2013) compared several parameterizations (including that of Woolf and Thorpe (1991)) and found discrepancies on the order of 50% between them. Therefore, we assume 50% uncertainty for the bubble injection correction (see e.g., Hull et al., 2016).

2.5.3. Vertical Entrainment

Waters underlying the mixed layer can be entrained into the mixed layer, consequently influencing mixed layer O_2 concentrations. The change in O_2 concentration from one time step to the next as the mixed layer deepens by Δh as determined by ITP density profiles can be expressed as

$$\Delta O_2^E = \frac{\Delta h}{h_t}(O_{2_{t-1}}^{sub} - O_{2_{t-1}}), \quad (8)$$

where $O_{2_{t-1}}^{sub}$ is the O_2 concentration of the waters being entrained into the mixed layer, defined as waters between h and $h + \Delta h$. Vertical entrainment of deeper waters only occurs when the mixed layer becomes deeper (i.e., $\Delta h > 0$), otherwise, $\Delta O_2^E = 0$. In some cases, the mixed layer depth can increase from one time step to the next as a result of water column heaving rather than vertical entrainment events. These heaving events (e.g., non-breaking internal waves) can be distinguished by examining the mixed-layer salinity changes, ΔS. In heaving events, $\Delta S = 0$. During entrainment events, for which mixed layers typically deepen by a few meters and average salinity gradients across the base of the mixed layer are on the order of 0.2, ΔS typically exceeds 0.06. Taking this as a threshold, we take $\Delta O_2^E = 0$ if $\Delta S < 0.06$. The uncertainty associated with ΔO_2^E is computed using the uncertainty of Δh, which is approximately 1 m.

2.5.4. Net Community Production

Biological processes including primary production and respiration can influence mixed-layer O_2 concentrations, although primary production requires sufficient light and nutrient availability, and respiration levels are low in cold wintertime waters (Sherr & Sherr, 2003). Estimations of net community production (NCP, the difference between rates of photosynthesis and respiration) give insight into the influence of biology on O_2 concentrations in the upper ocean. However, NCP remains difficult to quantify in the absence of information from, for example,

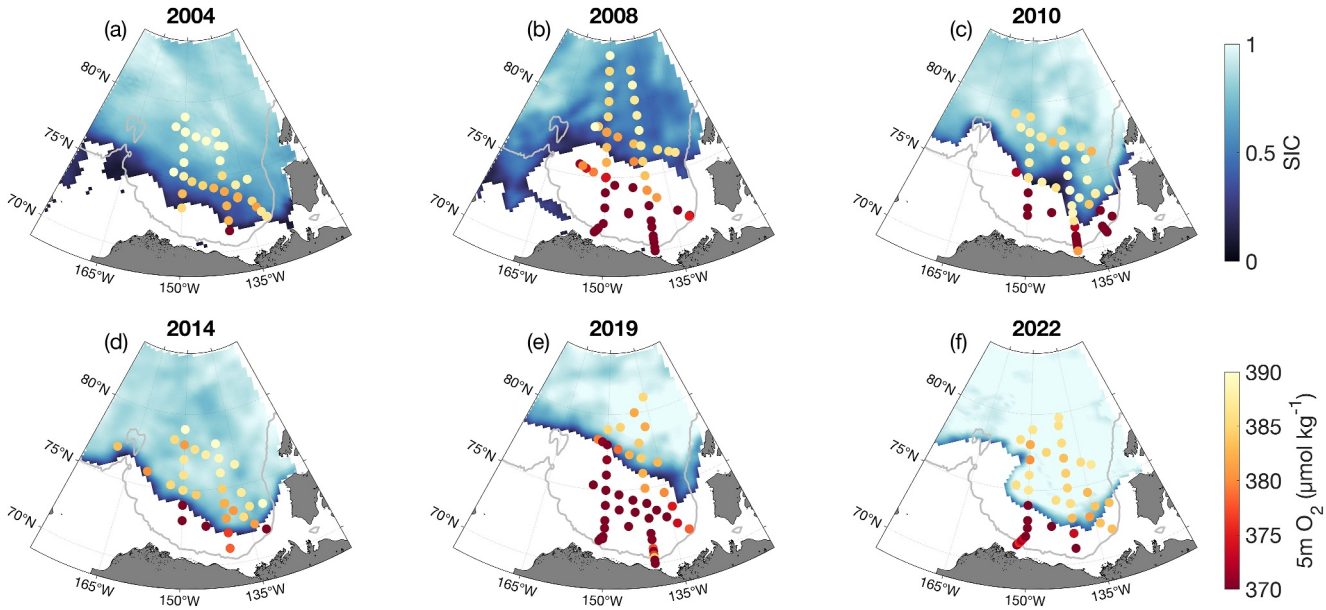

Figure 3. O_2 concentrations at 5 m depth from CTD/Rosette casts during the Joint Ocean Ice Study/Beaufort Gyre Observing System (JOIS/BGOS) expeditions are shown as colored dots for a subset of years (labeled at the top), underlain with the daily SIC from the midpoint (in time) of the expedition. SIC less than 0.05 are not plotted. The 500 m isobath is shown in gray. The analogous maps for all years between 2003 and 2022 are shown in Figure S2 in Supporting Information S1.

incubation experiments, $\Delta O_2/Ar$, nutrients, and chlorophyll-a concentrations. Due to data limitations, we do not compute changes in mixed layer O_2 concentrations due to NCP. Additionally, O_2 data shallower than those measured by the ITPs might be key in resolving O_2 signals resulting from biological processes. However, we discuss its potential contribution in context with our model results in Section 5.

2.5.5. Lateral Advection

In the Canada Basin, several studies have identified spatial variability attributed to surface ocean fronts which are characterized by transitions in physical and biogeochemical ocean properties (Eveleth et al., 2014; Islam et al., 2017; Timmermans et al., 2010). These horizontal property gradients suggest that lateral advection may influence the O_2 signal at any given location. In the context of observations made by the drifting ITPs, temporal change in O_2 could be attributed to lateral change in the surface ocean. For example, runoff from the Mackenzie River supplies the Canada Basin with fresh water, carrying an O_2 signature that likely reflects biological activity associated with the input of either nutrients or terrestrial organic matter to the region (e.g., Anderson et al., 2011). Although the one dimensional framework presented here cannot capture O_2 variability related to lateral processes, we identify these features by examining simultaneous transitions in mixed layer O_2, salinity, and temperature. In Section 5, we discuss the influence of spatial variability.

3. Spatial Distribution of Mixed Layer O_2

Processes influencing O_2 concentrations in the Canada Basin mixed layer are closely linked to the presence of sea ice cover. As a result, the sea ice extent in a given year typically sets up a spatial gradient in mixed-layer O_2 across the marginal ice zone, where the highest O_2 concentrations are generally observed under full sea ice cover, and the lowest O_2 concentrations are observed in ice-free open waters (Figure 3). It should be noted however that the 25 km by 25 km resolution passive microwave SIC field shown in Figure 3 is from the midpoint of the month-long hydrographic cruise over which time the marginal ice zone can change significantly. Mixed-layer O_2 concentrations typically decrease by approximately 15–20 µmol kg^{-1} from ice-covered to open water regions across the sea ice edge (Figure 3). Under-ice and open water O_2 concentrations are typically in the ranges of 380–400 and 350–370 µmol kg^{-1}, respectively. Note that mixed-layer O_2 concentrations near the Canada Basin margins (i.e., the shelf regions), which are generally more biologically productive due to availability of nutrients from river runoff and coastal upwelling, may differ significantly from central basin regions.

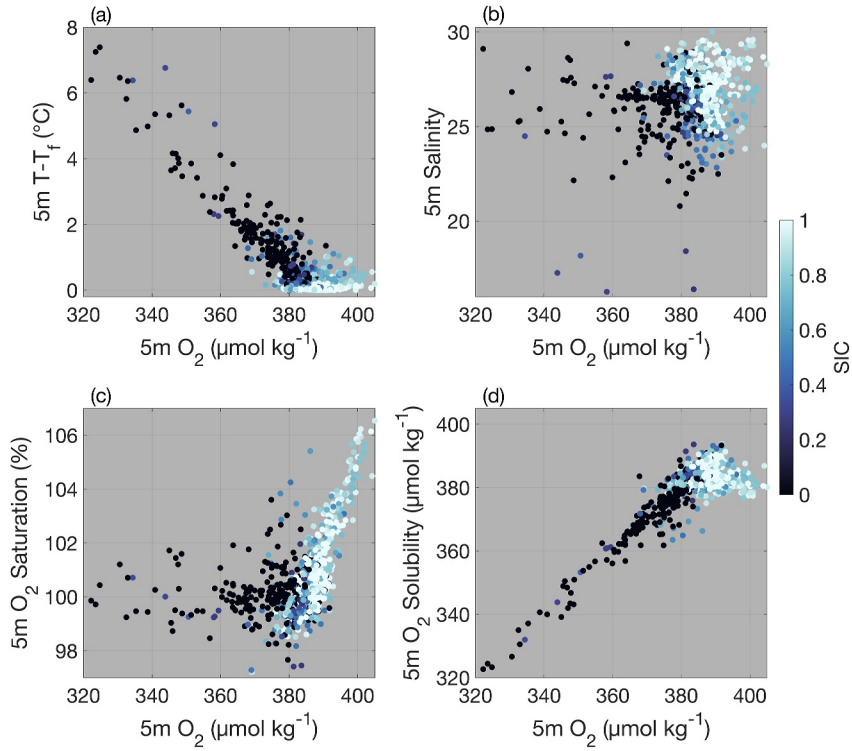

Figure 4. (a) The difference between the temperature and freezing point (T-T_f), (b) salinity, (c) O_2 percent saturation, and (d) O_2 solubility versus O_2, all measured at 5 m depth. Data are from CTD/Rosette casts during the annual JOIS/BGOS expeditions, and span 2003–2022. The dots are colored by SIC at the time and location of the CTD cast. To avoid O_2 measurements that could be influenced by biological activity near the shelf regions, the data shown here are limited to north of 71.9°N.

The relationships between O_2 and other mixed-layer properties (e.g., temperature, salinity, O_2 saturation, and O_2 solubility) strongly depend on the sea ice cover (Figure 4). In regions with low SIC, mixed-layer O_2 values are closely linked to mixed-layer temperatures (Figure 4a), due to the strong temperature dependence on O_2 solubility (Figure 4d). In low SIC regions O_2 percent saturation is generally near 100% (Figure 4c); small deviations from this may be where the ocean mixed layer has not yet equilibrated with the atmosphere. In the Arctic Ocean, equilibration times in open water regions are generally on the order of about 10–14 days (Eveleth et al., 2014), ranging primarily due to variations in wind speed and mixed-layer depth. In regions with high SIC, O_2 concentrations tend to exceed their solubility values (Figure 4d), resulting in super-saturation. Since sea ice cover typically inhibits air-sea gas exchange (e.g., Prytherch et al., 2017), it can be assumed that a mixed layer underlying full sea ice cover has been isolated from the atmosphere, and thus its O_2 concentrations have been influenced by processes other than air-sea exchange, including brine rejection/meltwater dilution, entrainment, and lateral advection.

Although there is no tight coupling between salinity and O_2 concentrations in the mixed layer, it is broadly the case that saltier and O_2 enriched mixed layers reside under high sea ice cover, while fresher mixed layers with lower O_2 tend to be associated with open water regions (Figure 4b). The lack of a significant correlation between mixed-layer salinity and O_2 concentrations is likely because surface ocean salinity and O_2 are sometimes influenced by different mechanisms (e.g., precipitation/evaporation, air-sea equilibration, and biological activity). Nonetheless, the pattern of high salinities and O_2 values under high SIC along with the tight positive coupling of O_2 and O_2 percent saturation under high sea ice cover (Figures 4b and 4c) suggest that super-saturation of mixed layer O_2 is linked to solute exclusion during sea ice formation. Having diagnosed spatial variability as it relates to sea ice cover, we now turn to examine temporal variations in mixed-layer O_2 in the following section.

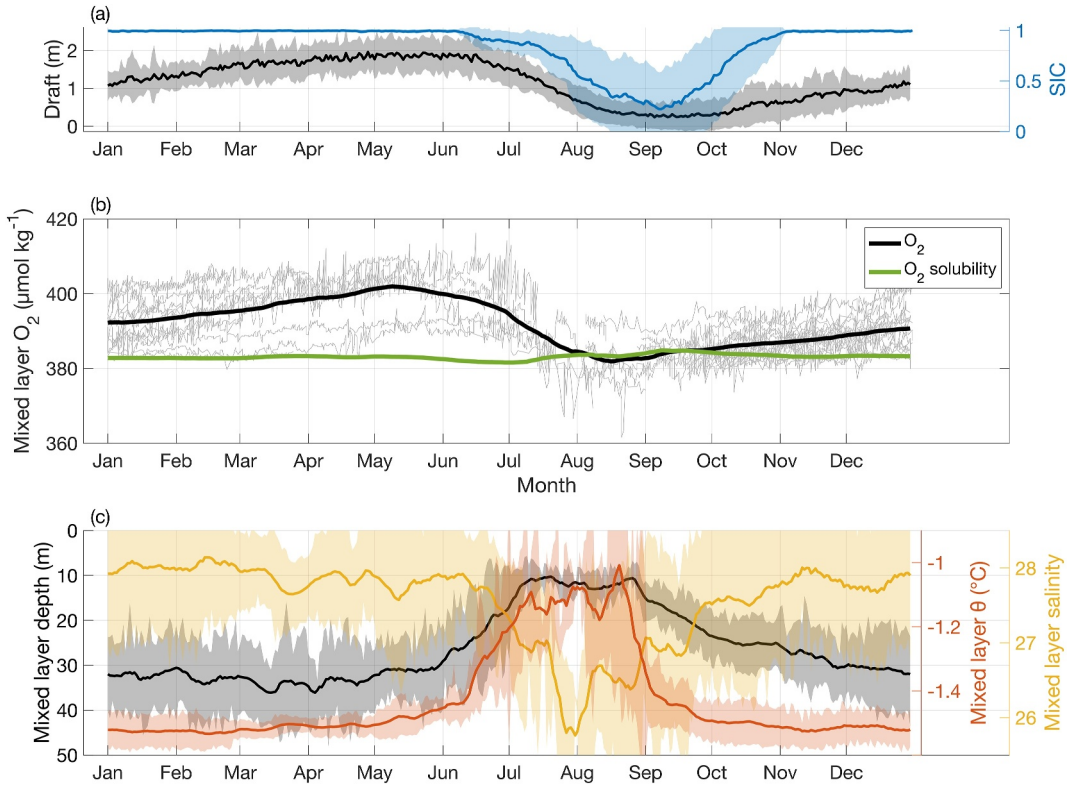

Figure 5. (a) Sea ice draft and concentration, averaged the locations of the 3 BGOS moorings between 2007 and 2019 are shown. The shading indicates one standard deviation. (b) The annual time series of mixed layer O_2 measured by 21 individual ITPs are shown in light gray, and the monthly running mean is shown in black. The monthly running mean of O_2 solubility is shown in green. (c) The seasonal evolution of mixed-layer depth, potential temperature, and salinity with weekly smoothing are shown. The shading indicates one standard deviation.

4. Seasonal Variability of Mixed Layer O_2 Linked to Ice Retreat

Given the spatial dependence of mixed layer O_2 concentrations on local sea ice extent in a given year (Figure 3), we investigate how seasonal variations in mixed layer O_2 are linked to seasonal sea-ice cycles and other mixed layer properties in the Canada Basin (Figure 5). The annual variations in mixed layer O_2 and sea ice draft in the Canada Basin are similar in structure ($R^2 = 0.94$), as both quantities gradually increase throughout late fall into early summer, then decline steeply to minima in late summer/early fall (Figures 5a and 5b), supporting that seasonal variability of O_2 is driven by processes related to sea ice growth and melt; note, however, that we will see in the following section that spatial variability sampled by the drifting ITPs may alias the seasonal evolution signal. The mixed layer is supersaturated ($O_{2sat} > 100\%$, i.e., O_2 concentrations exceed the solubility) throughout the ice growth season, and undersaturated ($O_{2sat} < 100\%$) in the melt season (Figure 5b). ITP data show that O_2 solubility remains relatively constant over the annual cycle (Figure 5b). For example, summer increases in solubility due to freshening tend to offset decreases due to warming (Figure 5c). As a result, there is an increase/decrease in O_2 saturation over the course of the ice growth/melt season when O_2 concentrations increase/decrease.

5. Model Results and Limitations

The one-dimensional model was run at a temporal resolution of one day ($\Delta t = 1$) using daily-averaged ITP measurements, atmospheric parameters (wind and SLP), and SIC from 21 ITPs equipped with O_2 sensors. Examples from two ITPs (ITPs 65 and 85) are presented for nearly a full annual cycle (Figures 6a–6f) in the respective years, and show that the sea-ice growth/melt term $\left(\Delta O_2^I\right)$ dominates over much smaller atmospheric flux and entrainment terms (ΔO_2^A and ΔO_2^E, respectfully). This suggests that the gradual increases in mixed layer O_2 throughout the late fall into early summer are primarily attributed to O_2 exclusion during sea ice growth, and

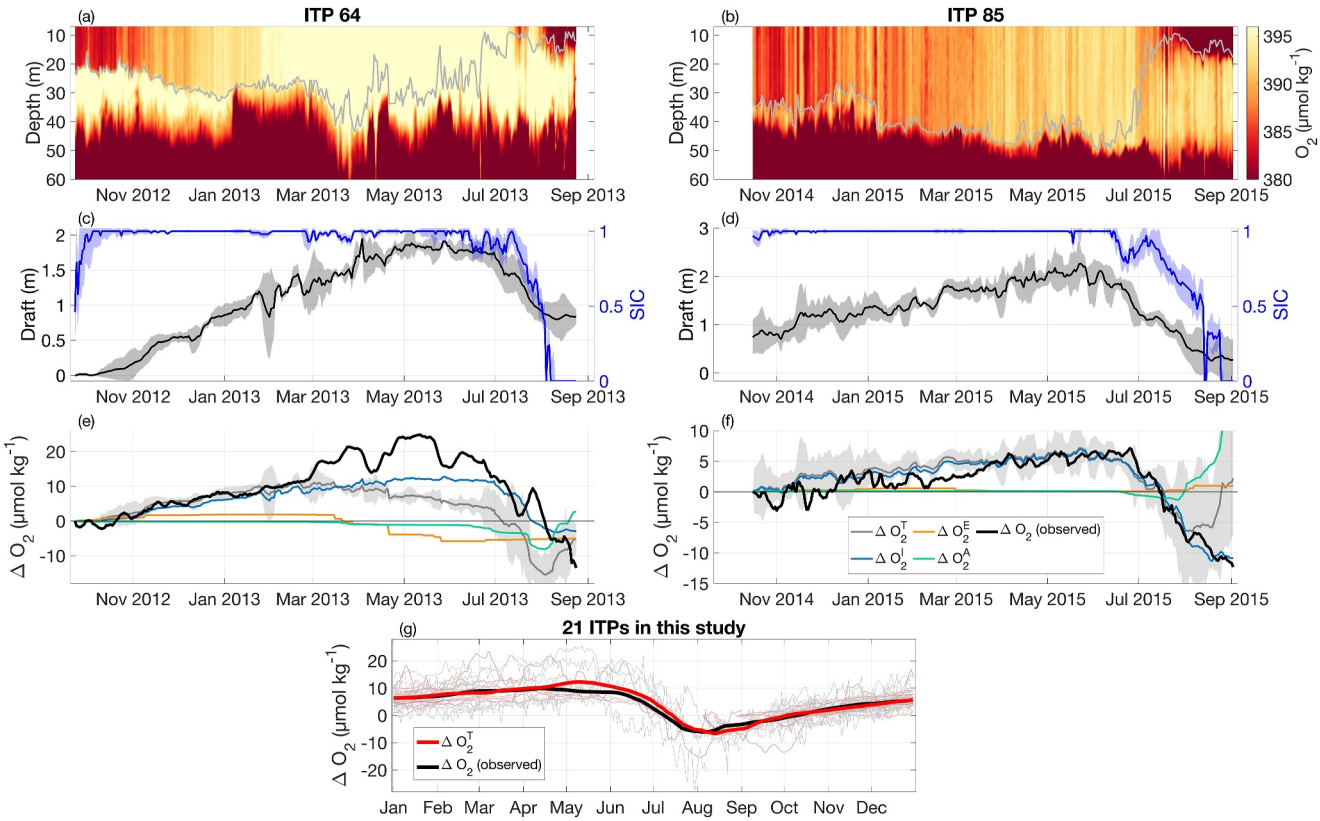

Figure 6. Model results and relevant parameters are shown for ITP 64 and 85: (a) and (b) depth-time plot of daily averaged O_2. The gray line represents mixed layer depth (see Section 2.2); (c) and (d) time series of sea ice draft and concentration, averaged in space (over the locations of the 3 BGOS moorings, see Figure 2a). The shading represents one standard deviation; (e) and (f) O_2 changes and model results (labeled) from each of the drivers are shown. The gray shading is the total model uncertainty (i.e., the sum of uncertainties from drivers). (g) The model results (ΔO_2^T, red lines) are compared to O_2 observations (black lines) for the 21 ITPs in this study. The thick red and black lines show monthly running averages of the model results and observations, respectively. Additional parameters for ITPs 64 and 85 are shown in Figures S3 and S4 in Supporting Information S1, respectively.

the sharp O_2 decreases throughout summer into early fall are likely driven by meltwater dilution. The modeled mixed-layer O_2 change $\left(\Delta O_2^T\right)$ generally captures the seasonal variability of O_2 as measured by the ITPs (Figure 6g).

Air-sea gas exchange is minimal throughout most of the year until ice cover begins to significantly decline (Figures 6e and 6f). During the ice growth season, sea ice cover typically prevents O_2 from escaping to the atmosphere, maintaining a super-saturated mixed layer. Spatial variability in SIC (e.g., lead openings) not resolved in the SIC product may give rise to localized regions of lower O_2 concentrations; these would not be captured here. In mid June to July when SIC decreases, there is typically a flux of O_2 out of the mixed layer (negative ΔO_2^A, green lines in Figures 6e and 6f), indicating outgassing of the excess O_2. In late July/early August when the mixed layer is slightly under-saturated due to meltwater dilution, the model shows a positive flux of O_2 into the mixed layer (see e.g., Rysgaard et al., 2011) which would persist until air-sea fluxes are once again inhibited by sea ice cover. However, this is not observed in the ITP O_2 records (Figures 6e and 6f), likely due to uncertainties associated with the wind and/or SIC data. Although the uncertainty provided with the ERA5 wind data is typically small (<1 m s^{-1}), we note that U_{10} computed from ERA5 reanalysis can differ by up to 5 m s^{-1} when compared with U_{10} from other products (i.e., NCEP/NCAR and NCEP/NARR), leaving room for a larger uncertainty than what is shown. Additionally, studies have noted uncertainties in the SIC data, specifically underestimations of SIC during sea ice melt and/or when the sea ice is thin (Ivanova et al., 2015; Kern et al., 2020). It is likely that due to these uncertainties, the modeled atmospheric flux is overestimated.

The contribution of vertical entrainment to seasonal O_2 variability varies in magnitude based on both the O_2 gradient between the mixed layer and underlying waters, and the extent of mixed layer deepening. The O_2

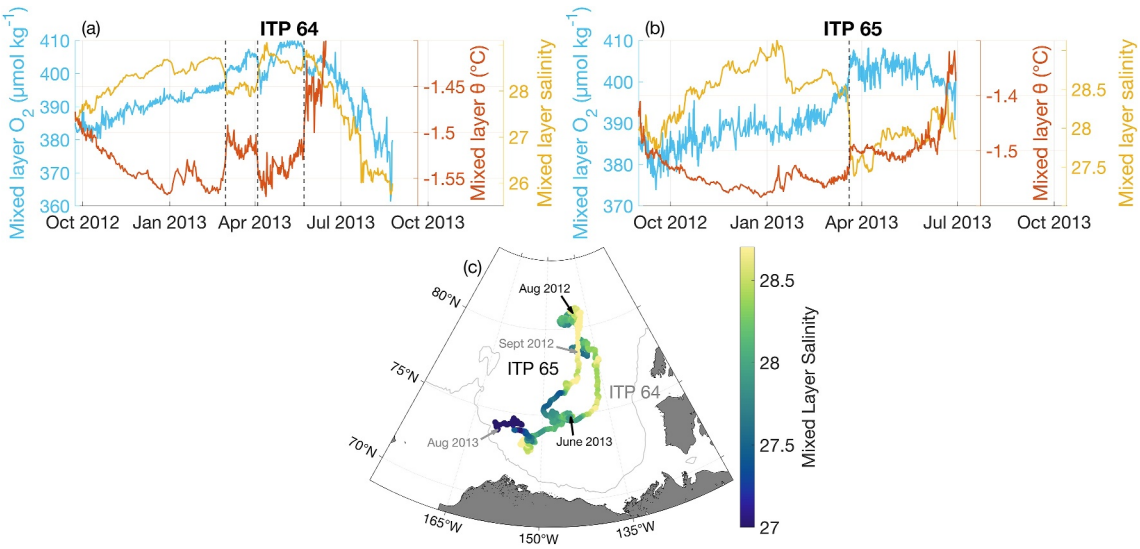

Figure 7. Time series of mixed-layer O_2, potential temperature, and salinity for (a) ITP 64 and (b) ITP 65. The abrupt changes in mixed layer properties, that is, front crossings, are marked by black dashed lines. (c) Map of ITP drift tracks (labeled) colored by mixed layer salinity. Gray and black arrows show the starting and ending locations (labeled by date) of ITPs 64 and 65, respectively. The 500 m isobath is shown in gray.

maximum beneath the mixed layer (Figures 1c and 6a-b) that is present from summertime until early-mid winter (Timmermans et al., 2010) results in positive ΔO_2^E during this period. Once this feature is mixed up, the waters beneath the mixed layer are O_2 depleted waters (originating from the Pacific Ocean) yielding negative ΔO_2^E throughout late winter into early summer. In some cases (e.g., ITP 85, Figure 6f), ΔO_2^E is effectively negligible, however, there are cases where ΔO_2^E contributes to O_2 variability which depending on the O_2 gradient across the mixed layer base and the extent of mixed layer deepening, as shown for the case of ITP 64 (Figure 6e). Although ITP 85 has a noticeable subsurface O_2 maximum (Figure 6b), it is much less pronounced than that observed in ITP 64 (Figure 6a), resulting in a weaker O_2 gradient across the mixed layer base. For this reason and likely due to some variations in mixed layer deepening, although the structure of ΔO_2^E for ITP 85 resembles that of ITP 64, it is an order of magnitude lower.

Processes that influence mixed layer O_2 but are not captured by the one-dimensional model (i.e., mainly lateral processes and NCP) potentially give rise to discrepancies between the modeled and observed O_2 concentrations. Due to the lack of sufficient light availability to support primary production from mid October through mid April in the Canada Basin (e.g., Laney et al., 2017), and considering minimal wintertime respiration (Sherr & Sherr, 2003) along with the lack of a decreasing O_2 signal in the ITP data, it is reasonable to assume negligible contributions of NCP to the O_2 budget during these months. Even during months with non-negligible solar radiation levels, the presence of sea ice cover can inhibit light levels, leading to no significant NCP O_2 fluxes (Islam et al., 2017). Although O_2 produced or consumed by biological processes could contribute to O_2 concentrations during months with sufficient light, we do not observe significant model discrepancies during these periods. Additionally, the strong seasonality of biological processes in the Arctic Ocean (i.e., primary production in the summer and respiration in the winter) would suggest increases in summertime O_2 and decreases in wintertime. However, observations show O_2 increases through the winter and decreases in the summer (Figure 5c). Altogether, this may suggest that NCP does not play an important role in driving O_2 changes here. Although the 21 ITP records and one-dimensional modeling results suggest biology is not playing a significant role within the region focused on in this study, this is not to suggest that the influence of biology should not be considered; in the future and in specific years and locations, particularly in the context of sea ice decline, these processes may play a crucial role.

The main discrepancy between modeled and observed O_2 change relates to times when the ITPs drifted across lateral fronts (see Timmermans et al., 2012) characterized by abrupt and coincident changes in O_2, salinity, and potential temperature (Figure 7). For example, mixed layer O_2 concentrations measured by ITP 64 show significant variability between March and June that is not captured by the modeled fluxes (Figure 6e). The presence

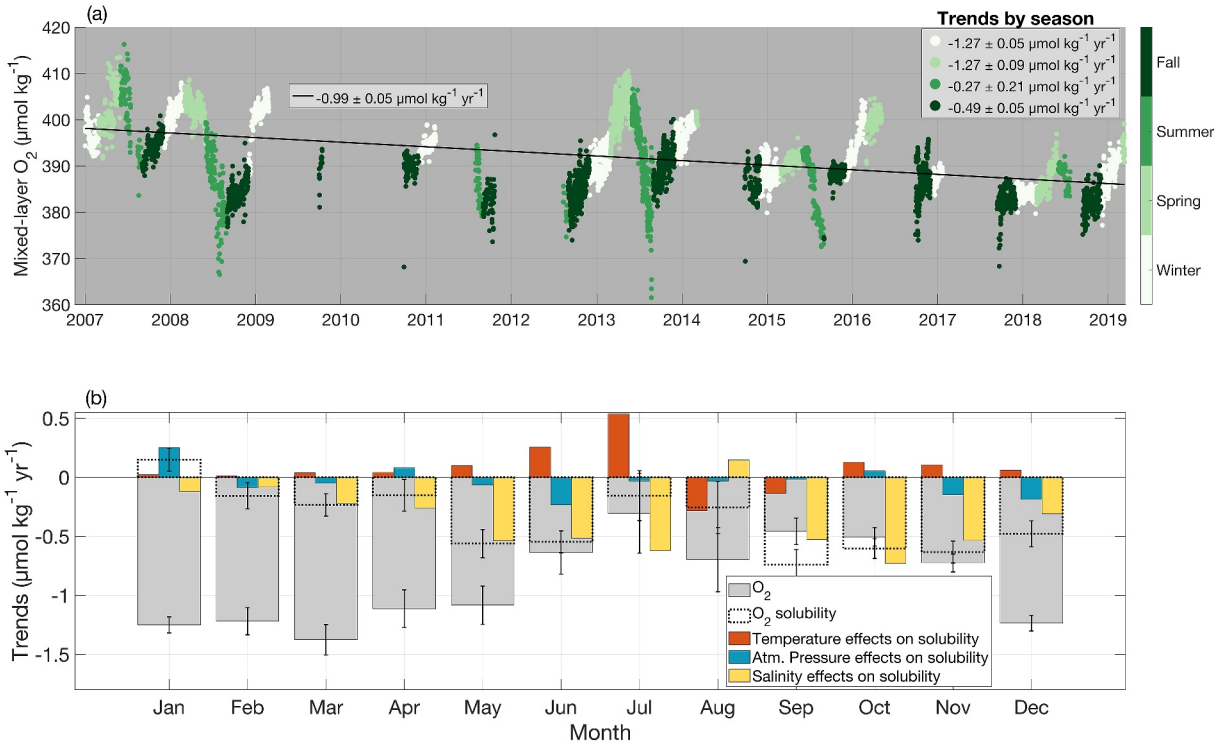

Figure 8. (a) Mixed-layer O_2 over time measured by 21 ITPs and hydrographic data, colored by season. The black line shows the linear trend (see legend). The linear trends for each season are also shown (labeled in legend). (b) Linear trends (and 95% confidence intervals on the linear fits) over 2007–2019 for O_2 and O_2 solubility (μmol kg^{-1} yr^{-1}) by month (gray and dashed bars, respectively), where the error bars indicate 95% confidence intervals on the linear fits. The contribution of temperature, atmospheric pressure, and salinity to the O_2 solubility trend are shown as thin orange, blue, and yellow bars, respectively. The number of ITP profiles in each season in each year is shown in Figure 2b.

of surface fronts are evident also in spatial variability of mixed-layer salinity that deviates from expectation of seasonal evolution (Figure 7c). Similarly, ITP 65 drifted across a surface front characterized by warm, fresh, and high O_2 waters in March (Figure 7b). Although spatial variability influences the time-series records of mixed-layer O_2 sampled by drifting ITPs, the contribution is generally minor compared to the seasonality driven by the annual cycle of sea ice growth and melt.

6. Interannual Variation in Mixed Layer O_2

Given the strong link between O_2 concentrations in the Canada Basin mixed layer and sea ice growth/melt, the obvious question becomes how O_2 concentrations relate to recent sea ice declines. To answer this, we consider interannual changes between 2007 and 2019 (the sampling duration of the 21 ITPs) for individual months. Over this period, mixed-layer O_2 concentrations declined at a rate of -0.99 ± 0.05 μmol kg^{-1} yr^{-1} (Figure 8a), however, we note this trend is likely biased due to the seasonal distribution of ITP and hydrographic measurements (Figure 2b). For this reason, trends by each season are also shown in Figure 8a, and we compute O_2 trends for each month (Figure 8b). Statistically significant decreases in mixed layer O_2 concentrations were observed in every month, with the most substantial decreases occurring in the months of December to May (Figure 8b). In most months, decreasing trends in O_2 solubility, primarily driven by mixed layer salinification, which Cole and Stadler (2019) attributed to changes in freshwater accumulation/storage, and slight decreases in atmospheric pressure were observed (Figure 8b). In September and October, the O_2 change is less than expected from changes in solubility alone, possibly suggesting some influence of increased primary production in recent years (e.g., Arrigo & van Dijken, 2015). In the remaining months the decrease in solubility only partially account for the decreasing O_2 trends. Throughout the winter months, the contribution of decreased solubility to the overall decreasing O_2 trend is minimal, and is much less than in other months, indicating that the mixed layer is becoming less saturated with respect to O_2 in more recent years ($-0.18 \pm 0.01\%$ yr^{-1}). The ULS ice-thickness estimates from the moorings indicate that the decrease in wintertime O_2 saturation cannot be attributed to reduced ice

growth over the record; note that this is consistent with the idea that a thinner ice pack is in fact associated with enhanced ice growth during winter in this region (e.g., Zhong et al., 2022). It is likely that the enrichment of O_2 in the mixed layer resulting from sea ice growth is decreasing due to some of the accumulated O_2 escaping the mixed layer through leads/areas of open water that are not resolved in the SIC data product.

7. Summary/Discussion

We provide strong evidence (Figures 3–6) that ice growth/melt cycles control the annual cycle of O_2 concentrations in the mixed layer of the Canada Basin. This is consistent with studies related to other gases in the Arctic mixed layer (e.g., pCO_2; DeGrandpre et al., 2019; Richaud et al., 2023). Observations from hydrographic and ITP data indicate higher O_2 under sea ice and lower O_2 concentrations under open water conditions. One-dimensional model results are compared to ITP observations, and reveal that mixed layer O_2 is primarily driven by solute exclusion and meltwater dilution during periods of sea ice growth and melt, respectively. Additional processes, including atmospheric gas exchange, vertical entrainment, and lateral advection generally play a much smaller role. Although the role of biology cannot be directly assessed without estimates of NCP, model results in context with observations, as well as the observed decreasing O_2 signal in summertime, would suggest biological processes do not dominate. Between 2007 and 2019, observed decreases in O_2 and O_2 saturation during winter months suggest increased outgassing of O_2 in wintertime likely due to reduced sea ice cover.

During winter months in the Canada Basin mixed layer, O_2 saturation is typically well above 100% (ranging from about 100 to 106% saturation), where thick and extensive sea ice cover typically inhibits outgassing to the atmosphere; the long-term decrease in O_2 trends hint at changes in the wintertime ice pack. Leads in the Arctic Ocean can play an important role in air-sea exchange (see e.g., Taylor et al., 2018), however, due to factors including coarse/sparse data coverage and cloud contamination (Hoffman et al., 2019; Qu et al., 2021), interannual trends in lead area using satellite imagery are difficult to quantify. Several studies have found increasing trends in sea ice drift speeds that cannot be primarily attributed to increased wind speeds (Kwok et al., 2013; Rampal et al., 2009; Zhang et al., 2022), suggesting lower internal ice stresses and more lead openings. We find that in winter-spring months, sea ice drift on average has increased by about 3.5 cm s^{-1} over the sample period (2007–2019) of the 21 ITPs (*cf.* Zhang et al. (2022) who reported an increase of about 4 cm s^{-1} in winter/spring over 1979–2019). While quantifying the exact open water area relating to leads is difficult, the increasing trends in sea ice drift speeds suggest a looser ice pack with more openings, which may account for increased air-sea exchange. Since decreasing O_2 in the mixed layer may be an indicator of evolving sea ice cover, continued research on under-ice O_2 dynamics can help us better understand how air-sea interactions may be evolving in a changing Arctic climate. Given that the structure of O_2 in the upper ocean is strongly linked to sea ice, O_2 measurements closer to the sea ice-ocean interface are required, and will provide important insights into how the processes governing the transfer of gases through the atmosphere-sea ice-ocean system are changing with sea ice decline.

Finally, it is useful to compare results here with mixed-layer O_2 seasonality in the mid-latitude ice-free oceans, where variability is driven by vertical entrainment, atmospheric exchange, and biological production/consumption (Wang et al., 2022). For example, O_2 concentrations in surface waters at the Bermuda Atlantic Time-series Study site vary by approximately 30–40 μmol kg^{-1} over an annual cycle (*cf.* ~20–30 μmol kg^{-1} sampled by ITPs in this study). This North Atlantic seasonal cycle is characterized by high wintertime O_2 due to high primary production rates, and low summertime O_2 resulting from lower primary productivity, atmospheric exchange and solar warming (Bates & Johnson, 2023). Similar to the decreasing trend of mixed-layer O_2 in wintertime found in this study (approximately −1.14 μmol kg^{-1} yr^{-1}), long-term decreasing trends in upper ocean O_2 concentrations have been observed globally (e.g., trends of around −0.31 μmol kg^{-1} yr^{-1} in the North Atlantic over 1983–2023, Bates & Johnson, 2023). Unlike the findings here for the Canada Basin mixed layer, O_2 reductions in mid-latitude regions have been attributed primarily to decreased solubility, reduced ventilation, and increased microbial respiration, all resulting from ocean warming (Breitburg et al., 2018; Helm et al., 2011; Schmidtko et al., 2017). In the analogous way that trends of declining O_2 in the mid latitudes are a clear indicator of climate change, the declining trend in Canada Basin mixed-layer O_2 that we speculate results from more openings in the wintertime ice pack, and therefore more efficient air-sea exchange, highlights a unique manifestation of Arctic climate change.

Data Availability Statement

The Ice-Tethered Profiler data were collected and made available by the Ice-Tethered Profiler Program based at the Woods Hole Oceanographic Institution (Krishfield et al., 2008; Toole et al., 2011) and are available at https://doi.org/10.7289/v5mw2f7x (Toole et al., 2016). The hydrographic and ULS mooring data were collected and made available by the NSF Beaufort Gyre Observing System (BGOS) (http://www.whoi.edu/beaufortgyre) in collaboration with researchers from Fisheries and Oceans Canada at the Institute of Ocean Sciences (IOS). ITP and BGOS data are also available at the NSF Arctic Data Center (https://arcticdata.io). Daily sea ice concentration data are available from the NOAA/NSIDC Climate Data Record of Passive Microwave Sea Ice Concentration, Version 4 via https://doi.org/10.7265/efmz-2t65 (Meier & Stewart, 2021). Wind and sea level pressure fields are from the ECMWF reanalysis data set (ERA5), and available from the Copernicus Climate Data Store at https://doi.org/10.24381/cds.adbb2d47 (Hersbach et al., 2020).

Acknowledgments
Funding for this study was provided by the National Science Foundation, Division of Polar Programs under Grant 1950077. Thanks to John Toole and the WHOI ITP program team. Special thanks to Sarah Zimmermann and colleagues at the Institute of Ocean Sciences for efforts with ship-based O_2 data collection and calibration.

References

Aagaard, K., Coachman, L., & Carmack, E. (1981). On the halocline of the Arctic Ocean. *Deep-Sea Research, Part A: Oceanographic Research Papers*, *28*(6), 529–545. https://doi.org/10.1016/0198-0149(81)90115-1

Anderson, L., Björk, G., Jutterström, S., Pipko, I., Shakhova, N., Semiletov, I., & Wåhlström, I. (2011). East Siberian Sea, an Arctic region of very high biogeochemical activity. *Biogeosciences*, *8*(6), 1745–1754. https://doi.org/10.5194/bg-8-1745-2011

Arrigo, K. R., & van Dijken, G. L. (2015). Continued increases in Arctic Ocean primary production. *Progress in Oceanography*, *136*, 60–70. https://doi.org/10.1016/j.pocean.2015.05.002

Arroyo, A., Timmermans, M.-L., Le Bras, I., Williams, W., & Zimmermann, S. (2023). Declining O_2 in the Canada Basin halocline consistent with physical and biogeochemical effects of Pacific Summer Water warming. *Journal of Geophysical Research: Oceans*, *128*(4), e2022JC019418. https://doi.org/10.1029/2022JC019418

Bates, N. R., & Johnson, R. J. (2023). Forty years of ocean acidification observations (1983–2023) in the Sargasso Sea at the Bermuda Atlantic time-series study site. *Frontiers in Marine Science*, *10*. https://doi.org/10.3389/fmars.2023.1289931

Belmonte Rivas, M., & Stoffelen, A. (2019). Characterizing ERA-Interim and ERA5 surface wind biases using ASCAT. *Ocean Science*, *15*(3), 831–852. https://doi.org/10.5194/os-15-831-2019

Breitburg, D., Levin, L. A., Oschlies, A., Grégoire, M., Chavez, F. P., Conley, D. J., et al. (2018). Declining oxygen in the global ocean and coastal waters. *Science*, *359*(6371), eaam7240. https://doi.org/10.1126/science.aam7240

Butterworth, B. J., & Miller, S. D. (2016). Air-sea exchange of carbon dioxide in the Southern Ocean and Antarctic marginal ice zone. *Geophysical Research Letters*, *43*(13), 7223–7230. https://doi.org/10.1002/2016GL069581

Cole, S. T., & Stadler, J. (2019). Deepening of the winter mixed layer in the Canada Basin, Arctic Ocean over 2006–2017. *Journal of Geophysical Research: Oceans*, *124*(7), 4618–4630. https://doi.org/10.1029/2019JC014940

Cox, G. F., & Weeks, W. F. (1983). Equations for determining the gas and brine volumes in sea-ice samples. *Journal of Glaciology*, *29*(102), 306–316. https://doi.org/10.3189/S0022143000008364

DeGrandpre, M. D., Lai, C.-Z., Timmermans, M.-L., Krishfield, R. A., Proshutinsky, A., & Torres, D. (2019). Inorganic carbon and pCO_2 variability during ice formation in the Beaufort Gyre of the Canada Basin. *Journal of Geophysical Research: Oceans*, *124*(6), 4017–4028. https://doi.org/10.1029/2019JC015109

Dmitrenko, I. A., Kirillov, S. A., Rysgaard, S., Barber, D. G., Babb, D. G., Pedersen, L. T., et al. (2015). Polynya impacts on water properties in a northeast Greenland fjord. *Estuarine, Coastal and Shelf Science*, *153*, 10–17. https://doi.org/10.1016/j.ecss.2014.11.027

Eveleth, R., Timmermans, M.-L., & Cassar, N. (2014). Physical and biological controls on oxygen saturation variability in the upper Arctic Ocean. *Journal of Geophysical Research: Oceans*, *119*(11), 7420–7432. https://doi.org/10.1002/2014JC009816

Falkner, K. K., Steele, M., Woodgate, R. A., Swift, J. H., Aagaard, K., & Morison, J. (2005). Dissolved oxygen extrema in the Arctic Ocean halocline from the North Pole to the Lincoln Sea. *Deep Sea Research Part I: Oceanographic Research Papers*, *52*(7), 1138–1154. https://doi.org/10.1016/j.dsr.2005.01.007

Garcia, H. E., & Gordon, L. I. (1992). Oxygen solubility in seawater: Better fitting equations. *Limnology & Oceanography*, *37*(6), 1307–1312. https://doi.org/10.4319/lo.1992.37.6.1307

Glud, R. N., Rysgaard, S., & Kühl, M. (2002). A laboratory study on O_2 dynamics and photosynthesis in ice algal communities: Quantification by microsensors, O_2 exchange rates, ^{14}C incubations and a pam fluorometer. *Aquatic Microbial Ecology*, *27*(3), 301–311. https://doi.org/10.3354/ame027301

Glud, R. N., Rysgaard, S., Turner, G., McGinnis, D. F., & Leakey, R. J. (2014). Biological-and physical-induced oxygen dynamics in melting sea ice of the Fram Strait. *Limnology & Oceanography*, *59*(4), 1097–1111. https://doi.org/10.4319/lo.2014.59.4.1097

Gordon, A., Chen, C., & Metcalf, W. (1984). Winter mixed layer entrainment of Weddell Deep Water. *Journal of Geophysical Research*, *89*(C1), 637–640. https://doi.org/10.1029/JC089iC01p00637

Helm, K. P., Bindoff, N. L., & Church, J. A. (2011). Observed decreases in oxygen content of the global ocean. *Geophysical Research Letters*, *38*(23), L23602. https://doi.org/10.1029/2011GL049513

Hersbach, H., Bell, B., Berrisford, P., Hirahara, S., Horányi, A., Muñoz-Sabater, J., et al. (2020). The ERA5 global reanalysis [Dataset]. *Quarterly Journal of the Royal Meteorological Society*, *146*(730), 1999–2049. https://doi.org/10.1002/qj.3803

Hoffman, J. P., Ackerman, S. A., Liu, Y., & Key, J. R. (2019). The detection and characterization of Arctic sea ice leads with satellite imagers. *Remote Sensing*, *11*(5), 521. https://doi.org/10.3390/rs11050521

Hull, T., Greenwood, N., Kaiser, J., & Johnson, M. (2016). Uncertainty and sensitivity in optode-based shelf-sea net community production estimates. *Biogeosciences*, *13*(4), 943–959. https://doi.org/10.5194/bg-13-943-2016

Islam, F., DeGrandpre, M. D., Beatty, C. M., Timmermans, M.-L., Krishfield, R. A., Toole, J. M., & Laney, S. R. (2017). Sea surface pCO_2 and O_2 dynamics in the partially ice-covered Arctic Ocean. *Journal of Geophysical Research: Oceans*, *122*(2), 1425–1438. https://doi.org/10.1002/2016JC012162

Ivanova, N., Pedersen, L. T., Tonboe, R., Kern, S., Heygster, G., Lavergne, T., et al. (2015). Inter-comparison and evaluation of sea ice algorithms: Towards further identification of challenges and optimal approach using passive microwave observations. *The Cryosphere*, *9*(5), 1797–1817. https://doi.org/10.5194/tc-9-1797-2015

Kern, S., Lavergne, T., Notz, D., Pedersen, L. T., & Tonboe, R. (2020). Satellite passive microwave sea-ice concentration data set inter-comparison for Arctic summer conditions. *The Cryosphere*, *14*(7), 2469–2493. https://doi.org/10.5194/tc-14-2469-2020

Körtzinger, A., Send, U., Wallace, D. W., Karstensen, J., & DeGrandpre, M. (2008). Seasonal cycle of O_2 and pCO_2 in the central Labrador Sea: Atmospheric, biological, and physical implications. *Global Biogeochemical Cycles*, *22*(1), GB1014. https://doi.org/10.1029/2007GB003029

Krishfield, R. A., Toole, J., Proshutinsky, A., & Timmermans, M.-L. (2008). Automated ice-tethered profilers for seawater observations under pack ice in all seasons. *Journal of Atmospheric and Oceanic Technology*, *25*(11), 2091–2105. https://doi.org/10.1175/2008JTECHO587.1

Kwok, R., Spreen, G., & Pang, S. (2013). Arctic sea ice circulation and drift speed: Decadal trends and ocean currents. *Journal of Geophysical Research: Oceans*, *118*(5), 2408–2425. https://doi.org/10.1002/jgrc.20191

Laney, S. R., Krishfield, R. A., & Toole, J. M. (2017). The euphotic zone under Arctic Ocean sea ice: Vertical extents and seasonal trends. *Limnology & Oceanography*, *62*(5), 1910–1934. https://doi.org/10.1002/lno.10543

Liang, J.-H., Deutsch, C., McWilliams, J. C., Baschek, B., Sullivan, P. P., & Chiba, D. (2013). Parameterizing bubble-mediated air-sea gas exchange and its effect on ocean ventilation. *Global Biogeochemical Cycles*, *27*(3), 894–905. https://doi.org/10.1002/gbc.20080

Lindsay, R., Wensnahan, M., Schweiger, A., & Zhang, J. (2014). Evaluation of seven different atmospheric reanalysis products in the Arctic. *Journal of Climate*, *27*(7), 2588–2606. https://doi.org/10.1175/JCLI-D-13-00014.1

Meier, F., & Stewart, J. S. (2021). NOAA/NSIDC climate data record of passive microwave sea ice concentration, version 4 [Dataset]. *National Snow and Ice Data Center*. https://doi.org/10.7265/efmz-2t65

Moreau, S., Kaartokallio, H., Vancoppenolle, M., Zhou, J., Kotovitch, M., Dieckmann, G. S., et al. (2015). Assessing the O_2 budget under sea ice: An experimental and modelling approach. *Elementa*, *3*, 000080. https://doi.org/10.12952/journal.elementa.000080

Owens, W. B., & Millard, R. C. (1985). A new algorithm for CTD oxygen calibration. *Journal of Physical Oceanography*, *15*(5), 621–631. https://doi.org/10.1175/1520-0485(1985)015<0621:ANAFCO>2.0.CO;2

Peralta-Ferriz, C., & Woodgate, R. A. (2015). Seasonal and interannual variability of pan-Arctic surface mixed layer properties from 1979 to 2012 from hydrographic data, and the dominance of stratification for multiyear mixed layer depth shoaling. *Progress in Oceanography*, *134*, 19–53. https://doi.org/10.1016/j.pocean.2014.12.005

Poisson, A., & Chen, C.-T. A. (1987). Why is there little anthropogenic CO_2 in the Antarctic bottom water? *Deep-Sea Research, Part A: Oceanographic Research Papers*, *34*(7), 1255–1275. https://doi.org/10.1016/0198-0149(87)90075-6

Prytherch, J., Brooks, I. M., Crill, P. M., Thornton, B. F., Salisbury, D. J., Tjernström, M., et al. (2017). Direct determination of the air-sea CO_2 gas transfer velocity in Arctic sea ice regions. *Geophysical Research Letters*, *44*(8), 3770–3778. https://doi.org/10.1002/2017GL073593

Qu, M., Pang, X., Zhao, X., Lei, R., Ji, Q., Liu, Y., & Chen, Y. (2021). Spring leads in the Beaufort Sea and its interannual trend using Terra/MODIS thermal imagery. *Remote Sensing of Environment*, *256*, 112342. https://doi.org/10.1016/j.rse.2021.112342

Rampal, P., Weiss, J., & Marsan, D. (2009). Positive trend in the mean speed and deformation rate of Arctic sea ice, 1979–2007. *Journal of Geophysical Research*, *114*(C5), C05013. https://doi.org/10.1029/2008JC005066

Richaud, B., Fennel, K., Oliver, E. C., DeGrandpre, M. D., Bourgeois, T., Hu, X., & Lu, Y. (2023). Underestimation of oceanic carbon uptake in the Arctic Ocean: Ice melt as predictor of the sea ice carbon pump. *The Cryosphere*, *17*(7), 2665–2680. https://doi.org/10.5194/tc-17-2665-2023

Richter-Menge, J. A., Perovich, D. K., Elder, B. C., Claffey, K., Rigor, I., & Ortmeyer, M. (2006). Ice mass-balance buoys: A tool for measuring and attributing changes in the thickness of the Arctic sea-ice cover. *Annals of Glaciology*, *44*, 205–210. https://doi.org/10.3189/172756406781811727

Rutgers van der Loeff, M. M., Cassar, N., Nicolaus, M., Rabe, B., & Stimac, I. (2014). The influence of sea ice cover on air-sea gas exchange estimated with radon-222 profiles. *Journal of Geophysical Research: Oceans*, *119*(5), 2735–2751. https://doi.org/10.1002/2013JC009321

Rysgaard, S., Bendtsen, J., Delille, B., Dieckmann, G. S., Glud, R. N., Kennedy, H., et al. (2011). Sea ice contribution to the air–sea CO_2 exchange in the Arctic and Southern Oceans. *Tellus B: Chemical and Physical Meteorology*, *63*(5), 823–830. https://doi.org/10.1111/j.1600-0889.2011.00571.x

Schmidtko, S., Stramma, L., & Visbeck, M. (2017). Decline in global oceanic oxygen content during the past five decades. *Nature*, *542*(7641), 335–339. https://doi.org/10.1038/nature21399

Sea-Bird Electronics Inc.,. (2018). Sea-bird electronics Inc., Inc. 2018. Verification methods for troubleshooting sea-bird dissolved oxygen sensors. Technical Note.

Sea-Bird Electronics Inc.,. (2023). Sea-bird electronics Inc., Inc. 2023. Application Note No. 64.

Sherr, B. F., & Sherr, E. B. (2003). Community respiration/production and bacterial activity in the upper water column of the central Arctic Ocean. *Deep Sea Research Part I: Oceanographic Research Papers*, *50*(4), 529–542. https://doi.org/10.1016/S0967-0637(03)00030-X

Taylor, P. C., Hegyi, B. M., Boeke, R. C., & Boisvert, L. N. (2018). On the increasing importance of air-sea exchanges in a thawing Arctic: A review. *Atmosphere*, *9*(2), 41. https://doi.org/10.3390/atmos9020041

Timmermans, M.-L., Cole, S., & Toole, J. (2012). Horizontal density structure and restratification of the Arctic Ocean surface layer. *Journal of Physical Oceanography*, *42*(4), 659–668. https://doi.org/10.1175/JPO-D-11-0125.1

Timmermans, M.-L., Krishfield, R. A., Laney, S., & Toole, J. (2010). Ice-tethered profiler measurements of dissolved oxygen under permanent ice cover in the Arctic Ocean. *Journal of Atmospheric and Oceanic Technology*, *27*(11), 1936–1949. https://doi.org/10.1175/2010JTECHO772.1

Toole, J. M., Krishfield, R., O'Brien, J. K., Houk, A. E., Cole, S. T., & Program, W. H. (2016). Ice-tethered profiler observations: Vertical profiles of temperature, salinity, oxygen, and ocean velocity from an ice-tethered profiler buoy system [Dataset]. *NOAA National Centers for Environmental Information*. https://doi.org/10.7289/v5mw2f7x

Toole, J. M., Krishfield, R. A., Timmermans, M.-L., & Proshutinsky, A. (2011). The ice-tethered profiler: Argo of the Arctic. *Oceanography*, *24*(3), 126–135. https://doi.org/10.5670/oceanog.2011.64

Toole, J. M., Timmermans, M.-L., Perovich, D. K., Krishfield, R. A., Proshutinsky, A., & Richter-Menge, J. A. (2010). Influences of the ocean surface mixed layer and thermohaline stratification on Arctic sea ice in the central Canada Basin. *Journal of Geophysical Research*, *115*(C10), C10018. https://doi.org/10.1029/2009JC005660

Top, Z., Martin, S., & Becker, P. (1985). On the dissolved surface oxygen supersaturation in the Arctic. *Geophysical Research Letters*, *12*(12), 821–823. https://doi.org/10.1029/GL012i012p00821

Wang, Z., Garcia, H. E., Boyer, T. P., Reagan, J., & Cebrian, J. (2022). Controlling factors of the climatological annual cycle of the surface mixed layer oxygen content: A global view. *Frontiers in Marine Science*, *9*, 1001095. https://doi.org/10.3389/fmars.2022.1001095

Wanninkhof, R. (2014). Relationship between wind speed and gas exchange over the ocean revisited. *Limnology and Oceanography: Methods*, *12*(6), 351–362. https://doi.org/10.4319/lom.2014.12.351

Woolf, D. K., & Thorpe, S. (1991). Bubbles and the air-sea exchange of gases in near-saturation conditions. *Journal of Marine Research*, *49*(3), 435–466. https://doi.org/10.1357/002224091784995765

Wu, Y., Bakker, D. C., Achterberg, E. P., Silva, A. N., Pickup, D. D., Li, X., et al. (2022). Integrated analysis of carbon dioxide and oxygen concentrations as a quality control of ocean float data. *Communications Earth & Environment*, *3*(1), 92. https://doi.org/10.1038/s43247-022-00421-w

Zhang, F., Pang, X., Lei, R., Zhai, M., Zhao, X., & Cai, Q. (2022). Arctic sea ice motion change and response to atmospheric forcing between 1979 and 2019. *International Journal of Climatology*, *42*(3), 1854–1876. https://doi.org/10.1002/joc.7340

Zhong, W., Cole, S. T., Zhang, J., Lei, R., & Steele, M. (2022). Increasing winter ocean-to-ice heat flux in the Beaufort Gyre region, Arctic Ocean over 2006–2018. *Geophysical Research Letters*, *49*(2), e2021GL096216. https://doi.org/10.1029/2021GL096216